JOURNAL OF SOLID STATE CHEMISTRY 90, 249–262 (1991)

Cluster Intergrowth of Perovskite and Defect Sodium Chloride Type Structures in the K–Nb–O System: The Structure of ~KNb_4O_6

GUNNAR SVENSSON

Department of Inorganic Chemistry, Arrhenius Laboratory, Stockholm University, S-10691 Stockholm, Sweden

Received July 11, 1990

A new reduced potassium niobate (~KNb_4O_6) of intergrowth type structure containing condensed Nb_6O_{12} clusters has been found. The structure has been determined from HREM images. The atomic positions have been refined with the Rietveld technique using X-ray powder diffraction data. The space group of KNb_4O_6 is $P4/mmm$; $Z = 1$, and its unit cell parameters are $a = 4.1393(1)$ and $c = 8.2537(2)$. ~KNb_4O_6 consists of alternating slabs of $KNbO_3$ (perovskite) and NbO (ordered deficient NaCl-type) both being a single unit thick. The structure is closely related to that of $A_2Nb_5O_9$ (A = Ba, Sr). Both phases can be considered as members ($n = 1$ and 2 respectively) of a homologous series $A_nNb_{3+n}O_{3+3n}$. Electron microscopy studies show the presence of defects, both as extra perovskite layers and missing NbO slabs, together with areas of more disordered intergrowth. The profile refinement and microanalysis of individual crystal fragments both indicate the structure to be niobium deficient according to the formula $K_{1+x/2}Nb_{4-x}O_6$.

Introduction

During the last few years a number of new reduced oxoniobates containing discrete or condensed Nb_6O_{12} clusters have been prepared. The Nb_6 octahedra in such clusters can be coordinated by oxygen atoms according to the scheme $Nb_6O_{12}{}^iO_6^a$ (Fig. 1a). There are thus 12 oxygen atoms (O^i) located outside the edges and 6 (O^a) located outside the apices of the Nb_6 octahedra. This notation can also be used to describe the connection pattern between octahedral clusters (*1*). Some examples of linkage are shown in Fig. 1b. The condensation of Nb_6O_{12} clusters normally occurs via corner-sharing. Three-dimensional condensation occurs in NbO and two-dimensional condensation in $A_2Nb_5O_9$ (A = Sr, Ba). NbO has a structure of ordered, deficient NaCl type (*2*) and can be described in terms of Nb_6O_{12} clusters, where the Nb_6 octahedra are linked by sharing corners throughout. The structure of $A_2Nb_5O_9$ is an intergrowth of slabs of perovskite type and slabs of NbO type (*3*). Dimers of corner-sharing Nb_6O_{12} clusters have recently been reported (*4*). Edge-sharing Nb_6O_{12} clusters have only been observed as isolated events in a disordered intergrowth between perovskite and NbO in phasoid regions of the Sr–Nb–O and Ba–Nb–O systems (*5*).

A new phase with condensed Nb_6O_{12} clusters has now been synthesized in the K–Nb–O system. Its structure is a homologue of that of $A_2Nb_5O_9$ and it has been determined by means of high-resolution electron microscopy (HREM). The atomic positions have been refined from X-ray powder patterns, using the Rietveld tech-

0022-4596/91 $3.00

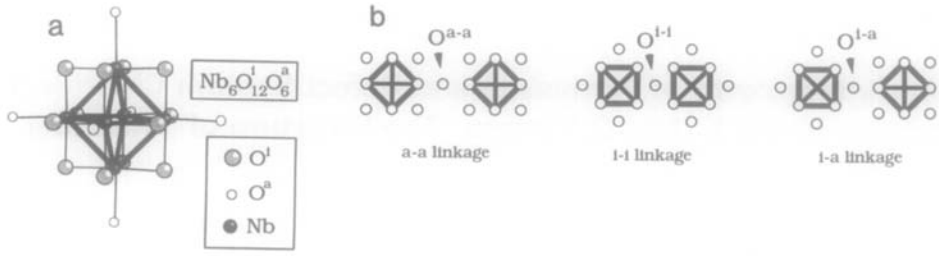

FIG. 1. (a) A $Nb_6O_{12}{}^iO_6{}^a$ cluster showing the O^i and O^a atoms. The former are located outside the edges, bonded to two Nb atoms in the same cluster, the latter outside the apices, bonded only to one Nb in the same cluster. (b) Examples of intercluster connections, O^{i-i}, O^{a-a} and O^{i-a} linkages.

nique. This paper will discuss the stoichiometry and structure of this phase as well as the great variety of defects observed with the electron microscope.

Experimental

The starting materials used were $KNbO_3$, Nb, and Nb_2O_5 (puriss 99.9% Roth Co.; purified from oxofluorides in air at 1100°C). $KNbO_3$ was prepared by heating K_2CO_3 (Baker's Analyzed) and Nb_2O_5 at 800°C for 15 hr, regrinding the product and heating it again for another 15 hr. NbO was obtained from mixtures of Nb_2O_5 and Nb heated at 1100°C for 18 hr in evacuated silica tubes. To obtain the monoxide as a single phase it was necessary to use a 13% excess of metal. This was probably due to an oxygen content of the niobium powder. The purity of the resulting phases was checked by examination of their X-ray powder diffraction patterns. In the case of NbO, the oxygen content was determined thermogravimetrically. Thoroughly ground mixtures of appropriate amounts of $KNbO_3$, Nb, and Nb_2O_5 or, alternatively, Nb, and NbO were heated at 1000°C in sealed Pt tubes placed in evacuated silica tubes. In some cases pressed tablets (3 × 6 mm) of the mixtures were used, wrapped in Nb foil and placed in evacuated silica tubes. After heat-treatment a dark product was obtained.

X-ray powder diffraction patterns were recorded in a focusing camera of the Guinier–Hägg type, using Cu$K\alpha_1$ radiation. Silicon (a = 3.525176 Å, (6)) was added as internal standard. The photographs were analyzed with a film-scanner measuring system (7). X-ray powder diffraction data for Rietveld refinement were collected with a STOE STADI/P powder diffractometer in symmetric transmission mode, using a small linear position-sensitive proportional counter (mini PSD) covering a 2θ range of approximately 4°. A curved Ge monochromator was used to obtain a focused Cu$K\alpha_1$ primary beam. The distance between the X-ray tube and the monochromator and between the monochromator and the detector was chosen to be 440 mm to provide sufficient angular resolution. Preferred-orientation effects were reduced by rapidly spinning the sample.

Elemental analysis of bulk material was carried out in a scanning electron microscope JEOL JSM-820 by means of a LINK energy-dispersive X-ray analysis system.

Transmission electron microscopy studies were made at 200 kV in JEOL JEM-200CX and JEM-2000FX microscopes. For this purpose small amounts of the samples were crushed in an agate mortar and dispersed in n-butanol. A drop of the dispersion was put on a holey carbon film supported by a copper grid. The HREM

micrographs were taken in the JEM-200CX microscope having a top-entry, double-tilt goniometer (±10°). The point-to-point resolution is 2.4 Å. The composition of individual crystal fragments was determined in the JEM-2000FX microscope with a LINK energy-dispersive detector in the high-angle (70°) position. Some HREM images were also taken in this microscope, which has a Scherzer resolution of about 3.1 Å.

Structure models obtained from the HREM micrographs were checked by image calculations based on the multislice method, using a locally modified version of the SHRLI suite (*8*).

Results

When the starting composition was $KNbO_3 \cdot xNbO$ (x = 1.5, 2, and 3) and Pt tubes were used as containers, no reaction seemed to occur. The X-ray patterns showed only the lines of $KNbO_3$ and NbO. In the tablets wrapped in Nb foil, only the outer parts seemed to have reacted. X-ray powder patterns of the inner parts showed only some weak extra reflections in addition to those of NbO and $KNbO_3$. The outer parts, however, gave strong lines from a new phase ($\sim KNb_4O_6$ see below) together with those of NbO. In some patterns very faint lines from another phase, believed to be KNb_8O_{14}, were observed.

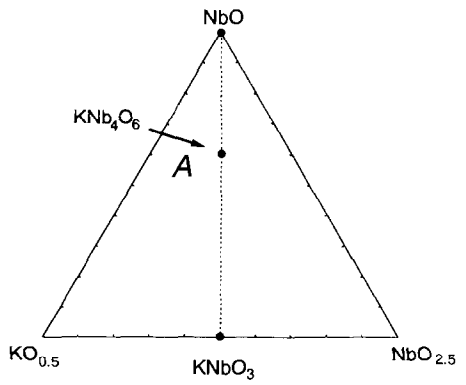

FIG. 2. A part of the composition diagram for the K–Nb–O system. The left side of the $KNbO_3$–NbO composition line is marked *A*.

TABLE I

CRYSTAL DATA FOR THE PROFILE REFINEMENT

Stoichiometry	$\sim KNb_4O_6$
Space group	*P4/mmm*
Z	1
F.W.	506.72
a/Å	4.1393(1)
c/Å	8.2537(2)
V/Å^3	141.42
d_{calc} (g/cm^3)	5.949

EDS analysis of the tablets confirmed these results. The inner parts of the tablets showed crystals with K/Nb ratios close to 1 or 0, obviously $KNbO_3$ and NbO. The outer parts contained crystals richer in niobium in addition to NbO. The total amount of this new phase, $\sim KNb_4O_6$, increased if the tablets were reground and reheated, but there were always strong lines from NbO present in the powder patterns.

At compositions on the left side (marked A in Fig. 2) of the $KNbO_3$–NbO composition line, $\sim KNb_4O_6$ was obtained also when Pt tubes were used as containers. However, lines from NbO were always present in the X-ray patterns, and very often also lines from $KNbO_3$. Diphasic samples of $\sim KNb_4O_6$ and NbO were only obtained on the reduced side of the $KNbO_3$–NbO composition line, i.e., the starting mixtures should contain a slight excess of niobium metal.

After excluding the NbO lines it was possible to index all the remaining reflections. The unit cell dimensions resulting from least-squares refinement are given in Table I. The indexed pattern is listed in Table II. The unit cell was confirmed by electron diffraction studies. In the ED patterns, streaking along [001] and twinning across (102) were frequently observed (see Fig. 3).

TABLE II

OBSERVED *d*-VALUES AND CALCULATED 2θ VALUES FOR THE GUINIER-HÄGG POWDER DIFFRACTION PATTERN OF ~KNb_4O_6 UP TO THE 21ST OBSERVED LINE

h k l	$2\theta_{calc}$	$\Delta(2\theta)$	d_{obs}(Å)	I_{obs}	I_{calc}
0 0 1	10.709	−0.027	8.275	1279	1290
1 0 0	21.445	−0.005	4.141	720	869
0 0 2	21.514			2	2
1 0 1	24.027			1	10
1 1 0	30.510			1	1
1 0 2	30.560	0.010	2.922	1532	1775
1 1 1	32.422	0.004	2.759	1390	1301
0 0 3	32.516			248	235
1 1 2	37.639	0.008	2.387	925	943
1 0 3	39.285	0.014	2.291	28	11
2 0 0	43.691	0.002	2.070	1557	1784
0 0 4	43.852	0.005	2.063	743	774
2 0 1	45.117			179	160
1 1 3	45.188	−0.002	2.005	491	403
2 1 0	49.167	0.003	1.851	185	193
2 0 2	49.201			1	1
1 0 4	49.301	0.018	1.846	171	185
2 1 1	50.474			0	10
2 1 2	54.255	0.004	1.689	689	762
1 1 4	54.348			1	1
2 0 3	55.506	0.008	1.654	247	166
0 0 5	55.628			6	4
2 1 3	60.192	0.001	1.536	21	16
1 0 5	60.309			10	8
2 2 0	63.502	0.087	1.462	569	568
2 0 4	63.615	−0.003		1091	1142
2 2 1	64.612	0.014	1.441	73	86
1 1 5	64.780	0.013	1.438	285	250
3 0 0	67.856			42	36
2 2 2	67.884			1	1
2 1 4	67.965	0.003	1.378	154	157
0 0 6	68.102			1	1
3 0 1	68.930			0	10
3 1 0	72.079			1	1
3 0 2	72.106	0.007	1.309	173	194
1 0 6	72.319	0.023	1.305	156	163
3 1 1	73.125	0.009	1.293	359	347

Note. $\Delta(2\theta) = 2\theta_{obs} - 2\theta_{calc}$. $\lambda = 1.5405981$ Å. Observed and calculated intensities are obtained from profile refinement using powder diffractometer data.

In an attempt to determine the composition of the new phase, EDS analysis was made in the transmission electron microscope. The compositions of the crystallites were determined from

$$C_{Nb}/C_K = k_{NbK} * I_{Nb(\lambda)}/I_{K(K)},$$

where C is the concentration of an element, I is the intensity of a characteristic X-ray line, and k is a constant determined from a standard, in the present case $KNbO_3$: $k_{NbK} = 0.66(3)$. This expression is valid in the thin-crystal limit, when absorption and fluorescence effects can be ignored (*9*). The average composition of 15 crystals of the new phase in a sample with nominal composition $K_2Nb_5O_9$ was found to be Nb/K = 3.2(3). The same result was obtained for a sample with the nominal composition $KNb_4O_{5.5}$. This is a significantly lower ratio than expected for KNb_4O_6, a fact that will be discussed below.

HREM images taken along the *a*-axis showed dark rows of crosses alternating with rows of lighter contrast (Fig. 4). The dark rows are very similar to the images of the NbO slabs found in the structures of $Ba_2Nb_5O_9$ (*3*) and $Sr_2Nb_5O_9$ (*10*). It appeared likely that the present structure was a similar intergrowth of NbO and perovskite type $KNbO_3$. The spacing of the dark rows is shorter, however, and corresponds to the homologue where the perovskite units are only a single unit cell wide instead of two units, as in $A_2Nb_5O_9$. The perovskite slabs thus share all their Nb atoms with the NbO units. The ideal composition of this structure is KNb_4O_6. The tetragonal lattices of KNb_4O_6 and $A_2Nb_5O_9$ can be described in terms of a cubic subcell where the *c*-axes are $c \approx 2c_{sub}$ and $c \approx 3c_{sub}$, respectively. Models of $A_2Nb_5O_9$ and KNb_4O_6 are compared in Fig. 5.

Structure Refinement

An X-ray powder pattern of a sample with the nominal composition $KNb_{3.5}O_{4.5}$ was chosen for Rietveld refinement. It contained reflections from ~KNb_4O_6 and NbO. The NbO reflections were relatively strong and the KNb_4O_6 lines rather broad, but there was no severe overlap between the

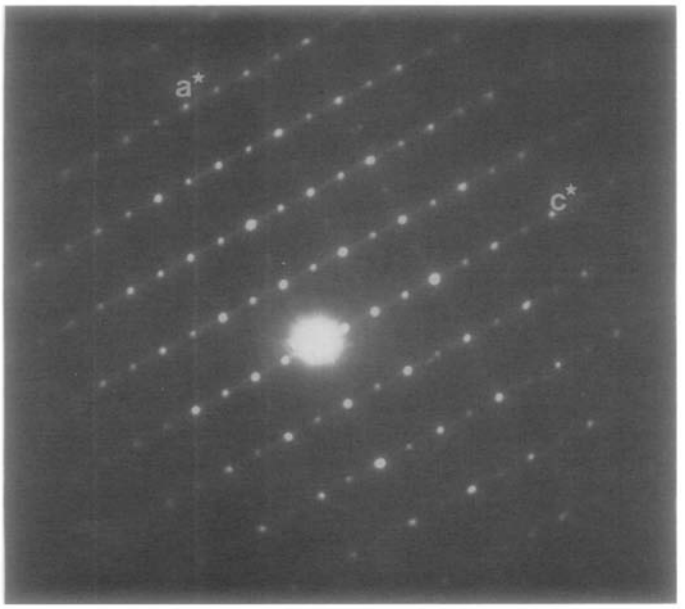

FIG. 3. ED pattern of ~KNb_4O_6 along the *a*-axis.

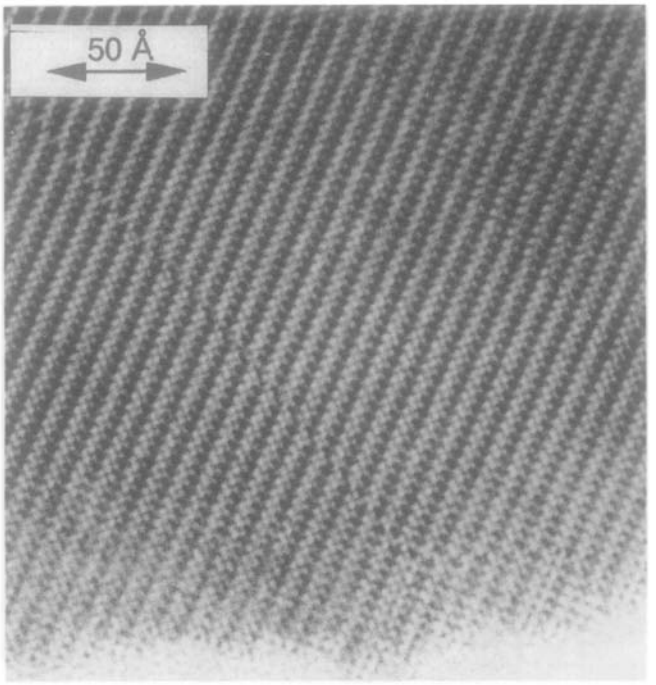

FIG. 4. HREM image of ~KNb_4O_6 along ⟨100⟩. The defocus was such that the dark rows of crosses in the image correspond to NbO slabs. Note that the crystal is slightly tilted, thereby giving a relief of the structure rather than a simple projection.

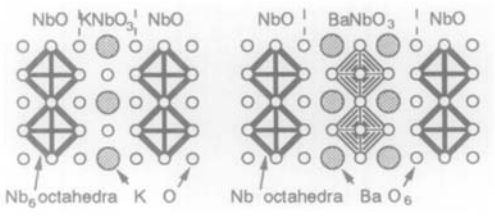

FIG. 5. Idealized structure models of KNb_4O_6 and $A_2Nb_5O_9$.

two sets of lines. Both phases were simultaneously refined. The starting set of atomic coordinates for KNb_4O_6 was obtained from the model shown in Fig. 5. The structure can be described in space group $P4/mmm$, which was used in the refinement.

The Rietveld program used was DBW3.2S (*11*). Step intensities in the range $7° < 2\theta < 87°$ were used in the refinement.

TABLE III

PARAMETERS FROM THE RIETVELD PROFILE REFINEMENT

No. of steps		4000	
Measured time (s/step)		160	
R_p		7.07	(6.59)
R_{wp}		9.46	(8.61)
	$\sim KNb_4O_6$		
No. of reflections		51	
No. of variables		12 or 13	
Profile parameters	U	= 0.268(18)	
	V	= −0.149(15)	
	W	= 0.043(3)	
	ass.	= 0.057	
R_I		8.70	(4.85)
R_F		6.24	(4.67)
	NbO		
No. of reflections (NbO)		14	
No. of variables (NbO)		8	
Profile parameters	U	= 0.051(9)	
	V	= −0.021(9)	
	W	= 0.012(2)	
	ass.	= 3.26	
R_I		3.38	(3.40)
R_F		1.78	(1.79)

Note. R-values within parentheses correspond to a refinement where the Nb(1) occupancy was allowed to vary.

A modified Lorentzian function was used for the representation of the individual reflection profiles. The angular dependence of the full-width at half maximum was assumed to be

$$(\mathrm{FWHM})^2 = U \tan^2\theta + V \tan\theta + W,$$

where U, V, and W are parameters to be refined. The parameters are given in Table III. The refinement was terminated when all shifts were less than 10% of the corresponding standard deviation. The final R-values were: for $\sim KNb_4O_6$, $R_F = 6.24\%$, and for NbO $R_F = 1.79\%$. The resulting positional parameters are given Table IV. Figure 6 shows the corresponding intensity profiles.

A refinement of the occupancy of Nb(1) resulted in a value of 88 ± 1% and a significantly lower R_F value: 4.68%, but the shifts in atomic positions were within the standard deviations. This Nb deficiency will be further discussed below. Refinements of the occupancy for the other atoms did not indicate any deviations from 100%. Negative temperature factors were obtained for both NbO and KNb_4O_6. This phenomenon is common when using data obtained with transmission geometry of Guinier type and is probably due to absorption in the sample. It is difficult to correct for the absorption

TABLE IV

ATOMIC COORDINATES FOR KNb_4O_6 (FULLY OCCUPIED) AND NbO OBTAINED FROM THE PROFILE REFINEMENT

Atom	Position	x/a	y/b	z/c	B(Å^2)	(occ.)
			$\sim KNb_4O_6$			
K	1(a)	0	0	0	−1.82	
Nb(1)	2(e)	0	0.5	0.5	−1.26	(0.88(1))
Nb(2)	2(h)	0.5	0.5	0.2405(5)	−1.26	
O(1)	1(c)	0.5	0.5	0	−2.20	
O(2)	4(i)	0.5	0	0.2348(18)	−2.20	
O(3)	1(b)	0	0	0.5	−2.20	
			NbO			
Nb	3(c)	0	0.5	0.5	−1.05	
O	3(d)	0.5	0	0	−1.50	

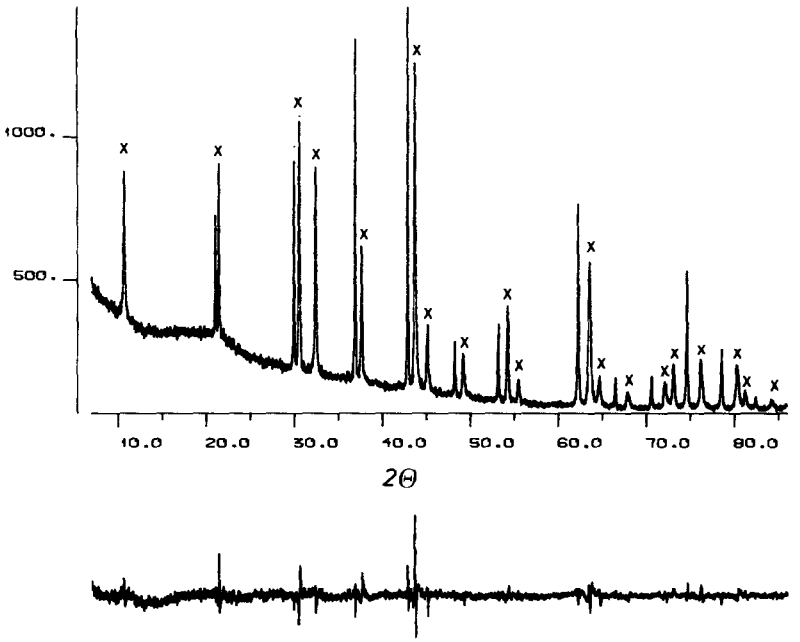

FIG. 6. Observed intensities (I_{obs}) and X-ray intensity differences ($I_{diff} = I_{obs} - I_{calc}$) for a sample with nominal composition $KNb_4O_{5.5}$. The peaks corresponding to $\sim KNb_4O_6$ are marked (X).

with this geometry, since the sample is not evenly distributed and its thickness is unknown.

Structure Description

A structure model of $\sim KNb_4O_6$ is shown in Fig. 7, and some selected interatomic distances are given in Table V. As mentioned above, the structure can be considered as an intergrowth of $KNbO_3$ and NbO. The K atoms are coordinated to 12 oxygen atoms as in the perovskite, forming a slightly distorted cubo-octahedron. Eight of

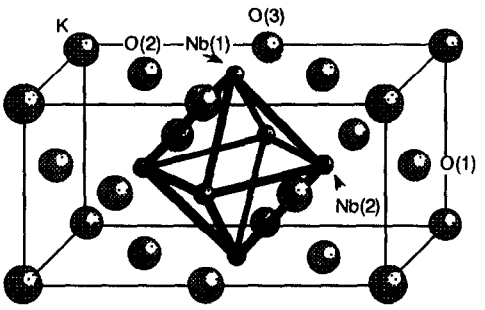

FIG. 7. Structure model of KNb_4O_6.

TABLE V

SELECTED INTERATOMIC DISTANCES (Å) WITH ESTIMATED STANDARD DEVIATIONS IN PARENTHESES

K(1) – 8*O(2)	2.867(10)
K(1) – 4*O(1)	2.927(—)
K(1) –8*Nb(2)	3.541(2)
Nb(1)– 2*O(3)	2.070(—)
Nb(1)– 2*O(2)	2.143(15)
Nb(1)–4*Nb(1)	2.927(—)
Nb(1)–4*Nb(2)	2.973(2)
Nb(2)– O(1)	1.992(3)
Nb(2)– 4*O(2)	2.071(—)
Nb(2)–4*Nb(1)	2.973(2)
Nb(2)– 4*K(1)	3.53841(2)
Nb(2)– Nb(2)	3.985(7)

the K–O distances are in the same range as in $KNbO_3$, 2.79–2.88 Å (*12*). The remaining four distances, K–O(1), are somewhat longer, 2.927 Å; this value being fixed by the length of the *a*-axis. This oxygen (O(1)) is also bonded to Nb(2), which is the Nb shared between the perovskite and the NbO units. This Nb–O bond is remarkably short: 1.992 Å. O(1) is positioned as an O^a atom relative to the Nb_6O_{12} cluster in the NbO slab. Such atoms are normally repelled by the O^i atoms in the cluster (*13*), and the Nb–O distances normally found are in the range 2.17–2.29 Å (*5*). This distance is instead rather close to the shortest Nb–O bonds found in orthorhombic $KNbO_3$: 1.991 Å (*12*).

The Nb(1)–Nb(1) distances (2.927 Å) in the Nb_6 octahedron are slightly shorter than the corresponding distances in $Ba_2Nb_5O_9$, while Nb(1)–Nb(2) is considerably longer (2.973 Å compared to 2.894 Å), close to the distance found in NbO (2.977 Å). The weakening of the four Nb–Nb bonds to Nb(2) is probably a compensation for the rather strong bond this atom forms to O(1).

Defects and Disorder

As mentioned above, streaking was frequently observed in the electron diffraction patterns. A HREM image of a part of such a crystalline is shown in Fig. 8. The main part is ordered KNb_4O_6, but disorder occurs frequently. In the more ordered area there are several traces of shear planes along {101}. Two types of shear vectors are present: [$\frac{1}{2}$**a**, 0, $\frac{1}{4}$**c**] and [0, 0, $\frac{1}{2}$**c**], marked A and B in Fig. 8. Models of these defects are shown in Fig. 9. The former shear seems to occur more frequently. A reason could be that in this case the Nb_6O_{12} clusters on different sides of the shear plane are linked via an O^{a-i} bridge and in the latter via an O^{i-i} bridge. In the Ba–Nb–O system the former bonding scheme has been found to be the most favorable (*5*).

Associated with these faults are other types of defects. Some of these are one-dimensional and others two-dimensional. The former occur as variations in the widths of the perovskite and NbO slabs. This type of disordered intergrowth has also been found in the Sr–Nb–O and Ba–Nb–O systems. In these systems a phasoid (*14*), designated α, has been found, with compositions in the area around $A_2Nb_9O_{14}$ and ANb_4O_6 (*5*). This phasoid has been discussed in terms of microphases and homologous series. The one-dimensional intergrowth found here, both the ordered (KNb_4O_6) and the disordered, is a member of one of these series with the general formula, $A_nNb_{n+3}O_{3+3n}$. In this series only the width of the perovskite slabs is allowed to vary. KNb_4O_6 and $A_2Nb_5O_9$ (A = Sr, Ba) are members with n = 1 and 2, respectively. In Figs. 8 and 10, defects corresponding to homologues with n = 2, 3, 4, and 5 can be found. Some of them are arrowed. The structures having n = 3 can be formed in the KNb_4O_6 structure by a simple replacement of the central Nb_2O layer in the NbO slabs by a KO layer (see E in Fig. 10). The remaining Nb atoms will become the centers of complete NbO_6 octahedra in perovskite-type slabs. A model of this is shown in Fig. 11a. If several adjacent NbO slabs are eliminated in this way, higher homologues with odd n values are obtained. For n = 2 and 4 the variation in n has to be accommodated by a shear along

FIG. 8. A typical HREM image of ~KNb_4O_6, showing both ordered and disordered areas. Note that the crystal is slightly tilted, thereby giving a relief of the structure rather than a simple projection. Two types of shear vectors are present: [$\frac{1}{2}$**a**, 0, $\frac{1}{4}$**c**] and [0, 0, $\frac{1}{2}$**c**] marked A and B. n = 2, 5, and 6 highlights one-dimensional defects being members of a homologues series with the general formula, $A_nNb_{n+3}O_{3+3n}$. (see text below)


200 Å
B
A
1
5
6
2
C

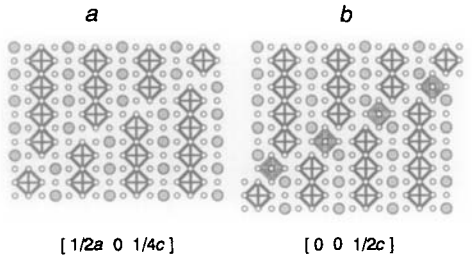

FIG. 9. Tentative models of the shear defects marked A and B in Fig. 8.

[0, 0, ½c], as shown in Fig. 11b. Variation in the width of the NbO layer does not occur frequently, but at the $n = 2$ defect in Fig. 8 a darkening in contrast (marked C) of one of the perovskite slabs can be seen. This can be interpreted as the replacement of the KO plane in the perovskite-type slab by an Nb_2O plane resulting in the formation of a double row of Nb_6 octahedra, as modeled in Fig. 12.

No large areas of two-dimensional intergrowth, as in the *A*–Nb–O systems, have been observed so far. NbO blocks that are limited in two dimensions do occur locally, however, in connection with the shear planes. In the image shown in Fig. 10, NbO blocks of sizes corresponding to 2 × 4, 2 × 2, and 1 × 4 NbO unit cells can be observed. This type of block has been discussed previously (*5*).

An important difference compared to the Ba and Sr systems is that the scattering power of the *A* cation is much smaller here. It is thus possible to distinguish between the potassium and the niobium atoms at most defocus values. At the defocus giving the optimum general contrast, which is the value normally chosen for imaging, the potassium atoms give no, or very faint, contrast, unlike the niobium atoms, which are clearly revealed as dark spots. In the Ba and Sr systems it was impossible to tell unambiguously directly from the images whether the perovskite structure was coherent throughout or if different regions were out-of-phase with respect to the *A* and Nb positions. This is not the case here. Moreover, the perovskite blocks are not entirely well-ordered but contain defects of various kinds, as can be seen in Fig. 10. An interpretation of the area marked D in Fig. 10 is shown in Fig. 13. In this model the NbO_6 octahedra share not only corners but also edges. As a consequence of this, larger cavities are created where the potassium atoms can be located. In both the cavities found in the interpreted part, a faint contrast can be seen slightly off-center, which could be due to potassium atoms.

Discussion

The inconsistency of the compositions determined by profile refinement and EDS analysis with that expected from the ideal structure model must be discussed. As mentioned above, defects and disorder occur relatively frequently. In Fig. 14 a typical crystal fragment containing several defects is shown. It is seen that some of the NbO slabs are missing, while others terminate within the structure. A majority of the NbO layers are separated by multiples of 8.3 Å, however, which is the length of the *c*-axis of KNb_4O_6. These defects can thus be created in an ideal KNb_4O_6 crystal by replacing the central Nb_2O layer in the NbO slab by a KO layer as descried above. If these defects occur in a random manner, the result on the average structure would just be a lowering of the scattering power on the Nb(1) position, as obtained from the X-ray diffraction data. The composition of the crystal would then vary as $K_{1+x/2}Nb_{4-x}O_6$, where x is the average number of Nb(1) atoms removed per unit cell. Using the Nb(1) occupancy, 88%, obtained from the refinement, an x value of 0.24 can be calculated. This gives an Nb/K ratio of 3.4. During the profile refinement the model discussed was tried. A refinement was made were the occupancies of the Nb(1)

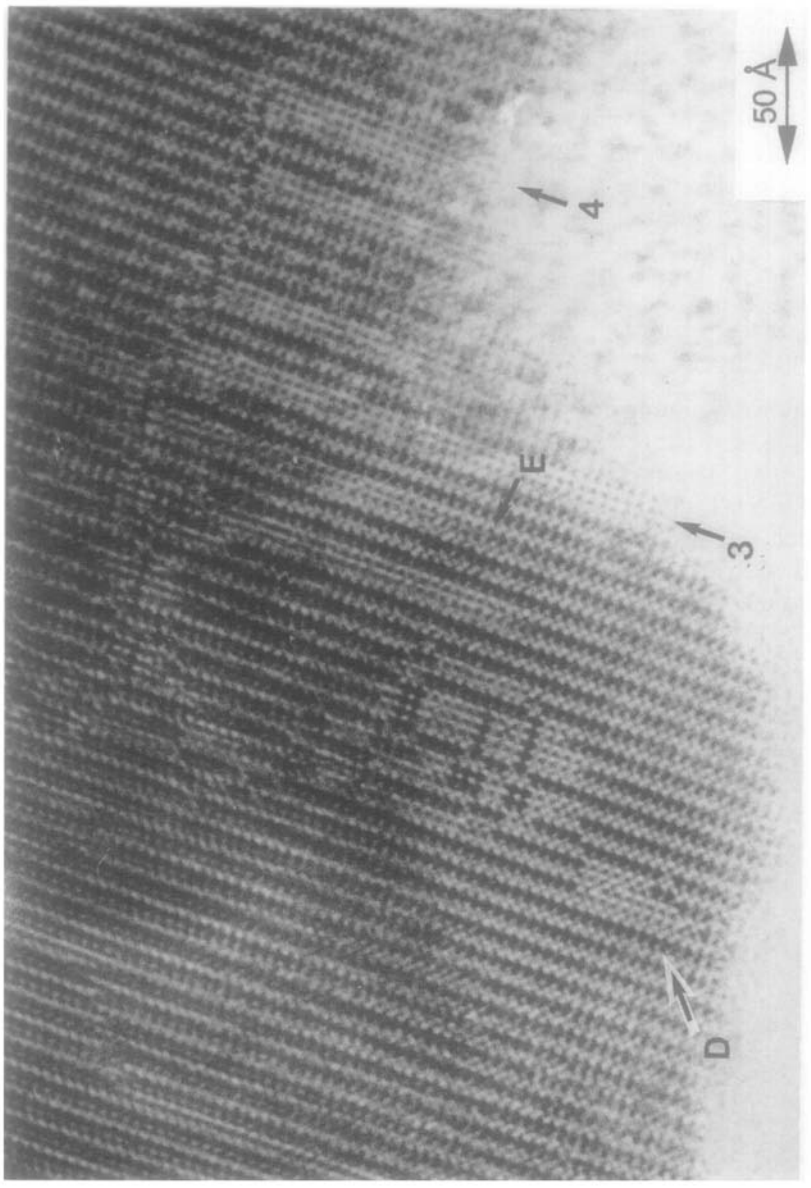

FIG. 10. An enlargement of the HREM image shown in Fig. 8. In the image variations of the perovskite slabs can be seen. This one-dimensional intergrowth corresponds to a homologous series with the general formula, $A_nNb_{n+3}O_{3n+3}$. In the figure, defects corresponding to homologues with $n = 3$ and 4 are marked. The area marked D is interpreted in Fig. 13 and E in Fig. 11a.

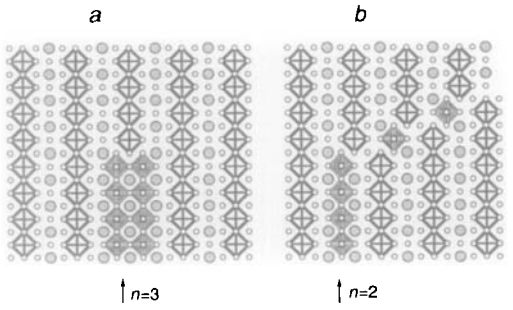

FIG. 11. Models showing how defects corresponding to homologues $n = 2$ and 3 can be accommodated in the structure. (a) An n odd can be formed by simply replacing the central Nb_2O in the NbO slabs by a KO layer (see E, Fig. 10). (b) Defects with n even must be accommodated by shear (e.g., [0, 0, ½c]).

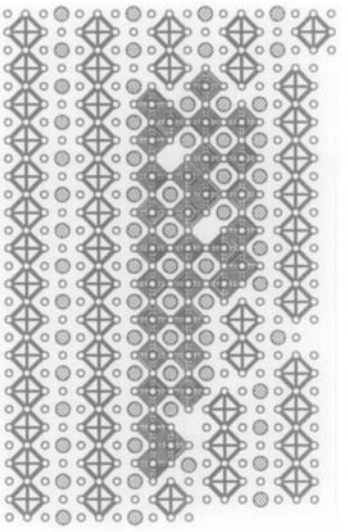

FIG. 13. Interpretation of the area marked D in Fig. 10. At the defocus giving the optimal general contrast, the K atoms give no or very faint contrast, unlike the niobium atoms, which are clearly revealed as dark spots. The model shown was constructed with due regard for this phenomenon. In the model, NbO_6 octahedra share not only corners but also edges.

and O(3) positions were coupled to the occupancy of a K site at (0, 0, 0.5) and an O site at (0.5, 0.5, 0.5). This resulted in an 88% occupancy for Nb(1) and O(3) and 12% for K and O, which also gives an x value of 0.24 and an Nb/K ratio of 3.4. The R_F-value was 5.7%. This model is thus not unreasonable, and the Nb/K ratios of 3.4 should be compared with the value 3.2(3) found by EDS analysis.

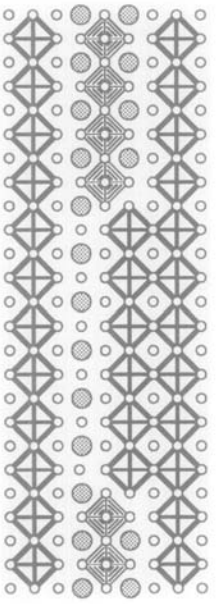

FIG. 12. Tentative model of C in Fig. 8 showing a defect with a variation in the width of the NbO layer.

The length of the a-axis of KNb_4O_6 is nearly the same as that of $Sr_2Nb_5O_9$ (see Table VI), but the latter has two perovskite units between the NbO slabs. This difference is probably not due to the slight differ-

TABLE VI

UNIT CELL PARAMETERS (Å) FOR Sr_xNbO_3 (*15*), $BaNbO_3$ (*15, 16*), $KNbO_3$ (*12*), $Ba_2Nb_5O_9$ (*3*), $Sr_2Nb_5O_9$ (*10*), AND $\sim KNb_4O_6$

	$BaNbO_3$	Sr_xNbO_3	$KNbO_3$
a =	4.085–4.095	3.985–4.025	5.697 ($\sqrt{2}$*4.028)
b =			3.971
c =			5.720 ($\sqrt{2}$*4.045)
	$Ba_2Nb_5O_9$	$Sr_2Nb_5O_9$	$\sim KNb_4O_6$
a =	4.1696	4.1405	4.1393
c =	12.228	12.040	8.2537
	(3*4.076)	(3*4.013)	(2*4.127)

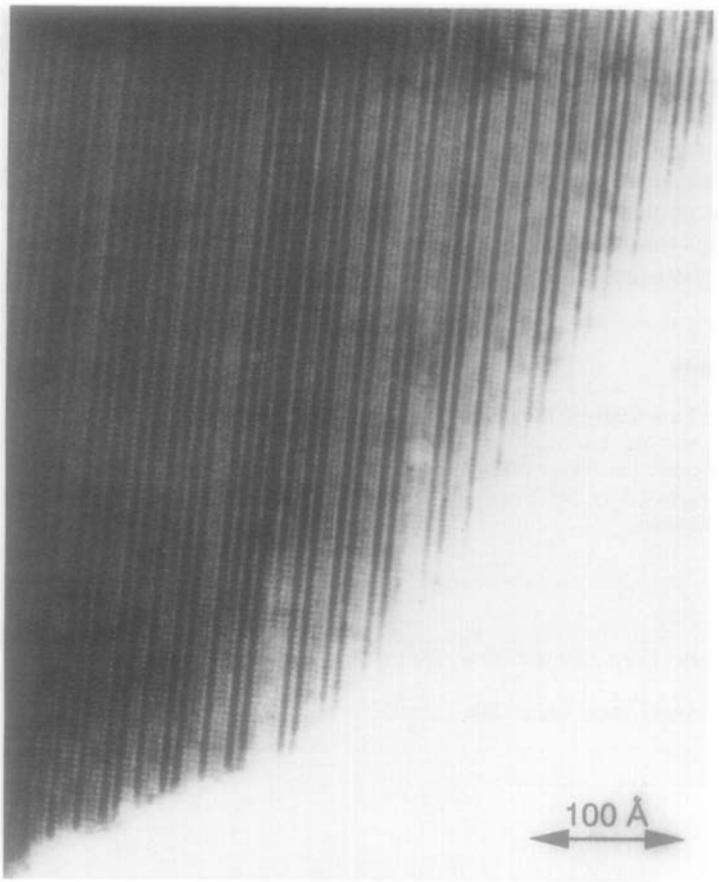

FIG. 14. HREM image from a typical fragment showing missing NbO slabs in ~KNb_4O_6. A majority of the NbO slabs are separated by multiples of 8.3 Å, which is the *c*-axis in KNb_4O_6. These defects can be created by replacing the central Nb_2O layer in the NbO slabs with a KO layer. If these defects occur in a random manner the result will just be a lowering of the scattering power of the Nb(1) position, as obtained from the X-ray diffraction data.

ence in size of the unit cells of the corresponding perovskites. The subcells in Sr_xNbO_3, $0.70 < x < 0.95$ (*15*), and $KNbO_3$ (*12*) are both ~4.0 Å; in the room temperature form of the latter, the octahedra are distorted. The main difference is the oxidation state of the niobium atom, in Sr_xNbO_3: +4.1–4.6 and in $KNbO_3$: +5. In $A_2Nb_5O_9$ (A = Sr, Ba) the niobium atom in the NbO_6 octahedron probably has an oxidation state between 4 and 5. This gives approximately 10 or 11 electrons for metal–metal bonding in the clusters, and a valence electron concentration (VEC) of 2.5–2.75 e^-/Nb. This should be compared with the values 2.33–2.67 found for discrete clusters (*1*) and 3.0 for the three-dimensional condensed clusters in NbO. Normally, the VEC is found to increase with the degree of condensation. In both KNb_4O_6 and the hypothetical phase $K_2Nb_5O_9$ there are 9 electrons for metal–metal bonding in the clusters, giving a maximum VEC of 2.25. In the hypothetical phase $K_2Nb_5O_9$, the niobium oxidation

state in the NbO_6 octahedra would be very close to +5. However, in such a phase there would probably be a charge transfer from the NbO slabs to the perovskite slab. This would decrease the already low VEC, thus making the structure less favorable. Anyhow, the large number of defects in the crystals indicates that the energy difference between the structures is rather low.

Acknowledgments

I thank Professor Lars Kihlborg for stimulating and helpful discussions and Mr. Lars Eriksson for assistance with the data collection. This work is a part of a research project supported by the Swedish Natural Science Research Council.

References

1. A. SIMON, *Angew. Chem. Int. Ed. Engl.* **27,** 159 (1988).
2. G. BRAUER, *Z. Anorg. Allg. Chem.* **248,** 1 (1941).
3. G. SVENSSON, *Mater. Res. Bull.* **23,** 437 (1988).
4. A. SIMON, J. KÖHLER, R. TISCHTAU, AND G. MILLER, *Angew. Chem.* **101,** 1695 (1989).
5. G. SVENSSON, *Chem. Commun. Univ. of Stockholm 1989,* No. 3.
6. C. R. HUBBARD, H. E. SWANSON, AND F. A. MAUER, *J. Appl. Crystallogr.* **8,** 45 (1975).
7. K. E. JOHANSSON, T. PALM, AND P.-E. WERNER, *J. Phys. E* **13,** 1298 (1980).
8. M. A. O KEEFE, *in* "Electron Optical system for microscopy, microanalysis and microlithiography, (J. J. Hren, F. A. Lenz, E. Munro, and P. B. Sewer, Eds.), SEM Inc., AMF O'Hare, IL (1984).
9. A. K. CHEETHAM AND A. J. SKARNULIS, *Anal. Chem.* **53,** 1060 (1981).
10. G. SVENSSON, *Acta Chem. Scand.* **44,** 222 (1990).
11. D. B. WILES AND R. A. YOUNG, *J. Appl. Crystallogr.* **14,** 1289 (1981).
12. L. KATZ AND H. D. MEGAW, *Acta Crystallogr.* **22,** 639 (1967).
13. J. KÖHLER AND A. SIMON, *Z. Anorg. Allg. Chem.* **553,** 106 (1987).
14. A. MAGNÉLI, *Chem. Scr.* **26,** 535 (1986).
15. D. RIDGLEY AND R. WARD, *J. Amer. Chem. Soc.* **77,** 6132 (1955).
16. G. SVENSSON AND P.-E. WERNER, *Mater. Res. Bull.* **25,** 9 (1990).